CMS Physics Analysis Summary

Contact: cms-pag-conveners-susy@cern.ch 2011/07/23

Search for new physics in events with opposite-sign dileptons and missing transverse energy

The CMS Collaboration

Abstract

A search is presented for physics beyond the standard model (SM) in final states with opposite-sign isolated lepton pairs accompanied by hadronic jets and missing transverse energy. Two complementary search strategies are performed using LHC data recorded at a center-of-mass energy $\sqrt{s} = 7$ TeV with the CMS detector, corresponding to an integrated luminosity of 0.98 fb^{-1}. The first search probes models with a specific dilepton production mechanism, which leads to a characteristic kinematic edge in the dilepton mass distribution. The second search probes models with heavy, colored objects which decay to final states including invisible particles, leading to very large hadronic activity and missing transverse energy. No evidence for an event yield beyond SM expectations is found. Upper limits on the non-SM contributions to the signal regions are deduced from the results, which are used to exclude a region of the parameter space of the constrained minimal supersymmetric extension of the standard model. Additional information related to detector efficiencies and response is provided to allow testing whether specific models of new physics are excluded by these results.

1 Introduction

In this note we describe a search for physics beyond the standard model (BSM) in a sample of proton-proton collisions at a centre-of-mass energy of 7 TeV. The data sample was collected with the Compact Muon Solenoid (CMS) detector [1] at the Large Hadron Collider (LHC) in 2011 and corresponds to an integrated luminosity of $0.98\,\text{fb}^{-1}$. This is an update of a previous analysis performed with a data sample of $34\,\text{pb}^{-1}$ collected in 2010 [2].

The BSM signature in this search is motivated by three general considerations. First, new particles predicted by BSM physics scenarios are expected to be heavy, since they have so far eluded detection. Second, BSM physics signals with high enough cross sections to be observed in our current dataset are expected to be produced strongly, resulting in significant hadronic activity. Third, astrophysical evidence for dark matter suggests [3, 4] that the mass of weakly-interacting massive particles is of the order of the electroweak symmetry breaking scale. Such particles, if produced in pp collisions, could escape detection and give rise to an apparent imbalance in the event transverse energy. We therefore focus on the region of high missing transverse energy ($E_{\text{T}}^{\text{miss}}$). An example of a specific BSM scenario is provided by R-parity conserving supersymmetric (SUSY) models in which new, heavy particles are pair-produced and subsequently undergo cascade decays, producing hadronic jets and leptons [5, 6]. These cascade decays may terminate in the production of weakly-interacting massive particles, resulting in large $E_{\text{T}}^{\text{miss}}$.

The results reported in this note are part of a broad program of BSM searches in events with jets and $E_{\text{T}}^{\text{miss}}$, characterized by the number and type of leptons in the final state. Here we describe a search for events containing opposite-sign isolated lepton pairs (e^+e^-, $e^\pm\mu^\mp$, $\mu^+\mu^-$) in addition to the jets and $E_{\text{T}}^{\text{miss}}$. Results from complementary searches with different final states have already been reported for example in Refs. [7, 8].

Our analysis strategy is as follows. In order to select dilepton events, we use high p_{T} dilepton triggers and a preselection based on that of the $t\bar{t}$ cross section measurement in the dilepton channel [9]. Good agreement is found between this data sample and predictions from standard model (SM) Monte Carlo (MC) simulations in terms of the event yields and shapes of various kinematic distributions. We search for a kinematic edge in the dilepton mass distribution, which is a characteristic feature of SUSY models in which the same-flavor opposite-sign leptons are produced via the decay $\chi_2^0 \to \ell\tilde{\ell} \to \chi_1^0\ell^+\ell^-$, where χ_2^0 is the next-to-lightest and χ_1^0 the lightest neutralino and $\tilde{\ell}$ is a slepton. Because BSM physics considered in this analysis is expected to have large hadronic activity and $E_{\text{T}}^{\text{miss}}$ as discussed above, we proceed to define 2 signal regions with requirements on these quantities to select about 0.1% of dilepton $t\bar{t}$ events, as predicted by MC. We perform counting experiments in these signal regions, and compare the observed yields with the predictions from two independent background estimation techniques based on data control samples, as well as with SM and BSM MC expectations. These 2 search approaches are complementary, since the dilepton mass edge search is sensitive to new physics models which do not have very large $E_{\text{T}}^{\text{miss}}$ and H_T, while the counting experiments do not assume a specific dilepton production mechanism and are also sensitive to new physics contributions which produce $e\mu$ lepton pairs.

No specific BSM physics scenario, e.g. a particular SUSY model, has been used to optimize the search. In order to illustrate the sensitivity of the search, a simplified and practical model of SUSY breaking, the constrained minimal supersymmetric extension of the standard model (CMSSM) [10, 11], is used. The CMSSM is described by five parameters: the universal scalar and gaugino mass parameters (m_0 and $m_{1/2}$, respectively), the universal trilinear soft SUSY breaking parameter A_0, the ratio of the vacuum expectation values of the two Higgs doublets ($\tan\beta$), and the sign of the Higgs mixing parameter μ. Throughout the note, three CMSSM

parameter sets, referred to as LM1, LM3 and LM6 [12], are used to illustrate possible CMSSM yields. The parameter values defining LM1 (LM3, LM6) are $m_0 = 60\ (330, 85)\ \text{GeV}/c^2$, $m_{1/2} = 250\ (240, 400)\ \text{GeV}/c^2$, $\tan\beta = 10\ (20, 10)$ GeV; all three parameter sets have $A_0 = 0$ and $\mu > 0$. These three scenarios are beyond the exclusion reach of previous searches performed at the Tevatron and LEP. The LM1 scenario was recently excluded by a search performed at CMS in events with jets and $E_{\mathrm{T}}^{\mathrm{miss}}$ [7]. In this analysis, the LM1, LM3 and LM6 scenarios serve as benchmarks which may be used to allow comparison of the sensitivity with other analyses.

2 CMS Detector

The central feature of the CMS apparatus is a superconducting solenoid, 13 m in length and 6 m in diameter, which provides an axial magnetic field of 3.8 T. Within the field volume are several particle detection systems. Charged particle trajectories are measured by silicon pixel and silicon strip trackers, covering $0 \leq \phi \leq 2\pi$ in azimuth and $|\eta| < 2.5$ in pseudorapidity, defined as $\eta = -\log[\tan\theta/2]$, where θ is the polar angle of the trajectory of the particle with respect to the counterclockwise proton beam direction. A crystal electromagnetic calorimeter and a brass/scintillator hadronic calorimeter surround the tracking volume, providing energy measurements of electrons and hadronic jets. Muons are identified and measured in gas-ionization detectors embedded in the steel return yoke outside the solenoid. The detector is nearly hermetic, allowing energy balance measurements in the plane transverse to the beam direction. A two-tier trigger system selects the most interesting pp collision events for use in physics analysis. A more detailed description of the CMS detector can be found elsewhere [1].

3 Event Selection

Samples of MC events are used to guide the design of the analysis. These events are generated using either the PYTHIA 6.4.22 [13] or MADGRAPH 4.4.12 [14] event generators. They are then simulated using a GEANT4-based model [15] of the CMS detector, and finally reconstructed and analyzed using the same software as is used to process collision data.

We apply a preselection based on that of the $t\bar{t}$ cross section measurement in the dilepton channel [9]. Events with two opposite-sign, isolated leptons (e^+e^-, $e^\pm\mu^\mp$, or $\mu^+\mu^-$) are selected. At least one of the leptons must have $p_{\mathrm{T}} > 20\,\text{GeV}/c$ and both must have $p_{\mathrm{T}} > 10\,\text{GeV}/c$, and the electrons (muons) must have $|\eta| < 2.5$ ($|\eta| < 2.4$). In events with more than two such leptons, the two leptons with the highest p_{T} are selected. Events with an e^+e^- or $\mu^+\mu^-$ pair with invariant mass between $76\,\text{GeV}/c^2$ and $106\,\text{GeV}/c^2$ or below $12\,\text{GeV}/c^2$ are removed, in order to suppress Drell–Yan (DY) $Z/\gamma^* \to \ell\ell$ events, as well as low mass dilepton resonances.

Events are required to pass at least one of a set of ee, $e\mu$ or $\mu\mu$ double-lepton triggers. The efficiency for events containing two leptons passing the analysis selection to pass at least one of these triggers is measured to be approximately 100%, 95%, and 90% for ee, $e\mu$ or $\mu\mu$ double-lepton triggers, respectively. In the following, the MC yields are weighted by these trigger efficiencies.

Because leptons produced in the decays of low-mass particles, such as hadrons containing b and c quarks, are nearly always inside jets, they can be suppressed by requiring the leptons to be isolated in space from other particles that carry a substantial amount of transverse momentum. The details of the lepton isolation measurement are given in Ref. [9]. In brief, a cone is constructed of size $\Delta R \equiv \sqrt{(\Delta\eta)^2 + (\Delta\phi)^2} = 0.3$ around the lepton momentum direction. The lepton relative isolation is then quantified by summing the transverse energy (as measured in

the calorimeters) and the transverse momentum (as measured in the silicon tracker) of all objects within this cone, excluding the lepton, and dividing by the lepton transverse momentum. The resulting quantity is required to be less than 0.15, rejecting the large background arising from QCD production of jets.

We require the presence of at least two jets with $p_{\mathrm{T}} > 30\,\mathrm{GeV}/c$ and $|\eta| < 3.0$, separated by $\Delta R > 0.4$ from leptons passing the analysis selection with $p_{\mathrm{T}} > 10\,\mathrm{GeV}/c$. The anti-$k_T$ clustering algorithm [16] with $\Delta R = 0.5$ is used for jet clustering. The jets and $E_{\mathrm{T}}^{\mathrm{miss}}$ are reconstructed with the Particle Flow technique [17]. The event is required to satisfy $H_{\mathrm{T}} > 100\,\mathrm{GeV}$, where H_{T} is defined as the scalar sum of the transverse energies of the selected jets. In addition, the $E_{\mathrm{T}}^{\mathrm{miss}}$ in the event is required to exceed 50 GeV.

The data yields and corresponding MC predictions after this event preselection are given in Table 1. The MC yields are normalized to $0.98\,\mathrm{fb}^{-1}$ using next-to-leading order (NLO) cross sections. At the current LHC luminosity, the mean number of interactions in a single beam crossing is approximately 5. In the MC, multiple interactions are superimposed on the hard collision, and the MC is reweighted such that the distribution of reconstructed primary vertices matches that in data. As expected, the MC predicts that the sample passing the preselection is dominated by dilepton $t\bar{t}$. The data yield is in reasonable agreement with the prediction. We also quote the yields for the LM1, LM3 and LM6 benchmark scenarios.

Table 1: Data yields and MC predictions after preselection, using the quoted NLO production cross sections σ. The $t\bar{t} \to \ell^+\ell^-$ corrresponds to dilepton $t\bar{t}$, including $t \to W \to \tau \to \ell$; $t\bar{t} \to$ fake includes all other $t\bar{t}$ decay modes. The samples of MC $t\bar{t}$, $W^{\pm}$ + jets, and single-top events were generated with MADGRAPH. The Drell–Yan sample (which includes events with invariant masses as low as $10\,\mathrm{GeV}/c^2$) was generated using a mixture of MADGRAPH and PYTHIA and includes decays to the $\tau^+\tau^-$ final state. All other samples were generated with PYTHIA. The LM1, LM3 and LM6 benchmark scenarios are defined in the text; the quoted σ values refer to the total production cross section for SUSY particles in these scenarios. Uncertainties are statistical only.

Sample	σ [pb]	ee	$\mu\mu$	$e\mu$	total
$t\bar{t} \to \ell^+\ell^-$	17	412.8 ± 8.9	465.4 ± 9.0	1095.6 ± 14.2	1973.8 ± 19.0
$t\bar{t} \to$ fake	141	12.6 ± 1.6	3.7 ± 0.8	22.7 ± 2.0	39.0 ± 2.7
DY$\to \ell^+\ell^-$	16677	18.6 ± 5.0	26.6 ± 6.0	37.6 ± 7.1	82.8 ± 10.6
W^+W^-	43	4.0 ± 0.5	4.3 ± 0.4	9.5 ± 0.7	17.7 ± 0.9
$W^{\pm}Z^0$	18	0.8 ± 0.1	1.0 ± 0.1	1.9 ± 0.1	3.8 ± 0.2
Z^0Z^0	5.9	0.3 ± 0.0	0.4 ± 0.0	0.4 ± 0.0	1.2 ± 0.1
single top	102	12.6 ± 0.6	14.0 ± 0.6	33.2 ± 1.0	59.9 ± 1.3
W + jets	96648	12.6 ± 5.4	0.0 ± 0.0	7.8 ± 4.6	20.5 ± 7.1
total SM MC		474.5 ± 11.7	515.4 ± 10.8	1208.6 ± 16.7	2198.5 ± 23.1
data		524	576	1381	2481
LM1	6.7	62.3 ± 1.6	69.5 ± 1.6	35.8 ± 1.2	167.5 ± 2.6
LM3	5.3	22.1 ± 0.8	26.9 ± 0.9	39.7 ± 1.1	88.6 ± 1.7
LM6	0.5	4.5 ± 0.1	5.0 ± 0.1	5.7 ± 0.1	15.3 ± 0.2

Figure 1 compares several kinematic distributions in data and SM MC for events passing the preselection. As an illustration, we also show the MC distributions for the LM6 benchmark point. We find that the SM MC reproduces the properties of the bulk of data.

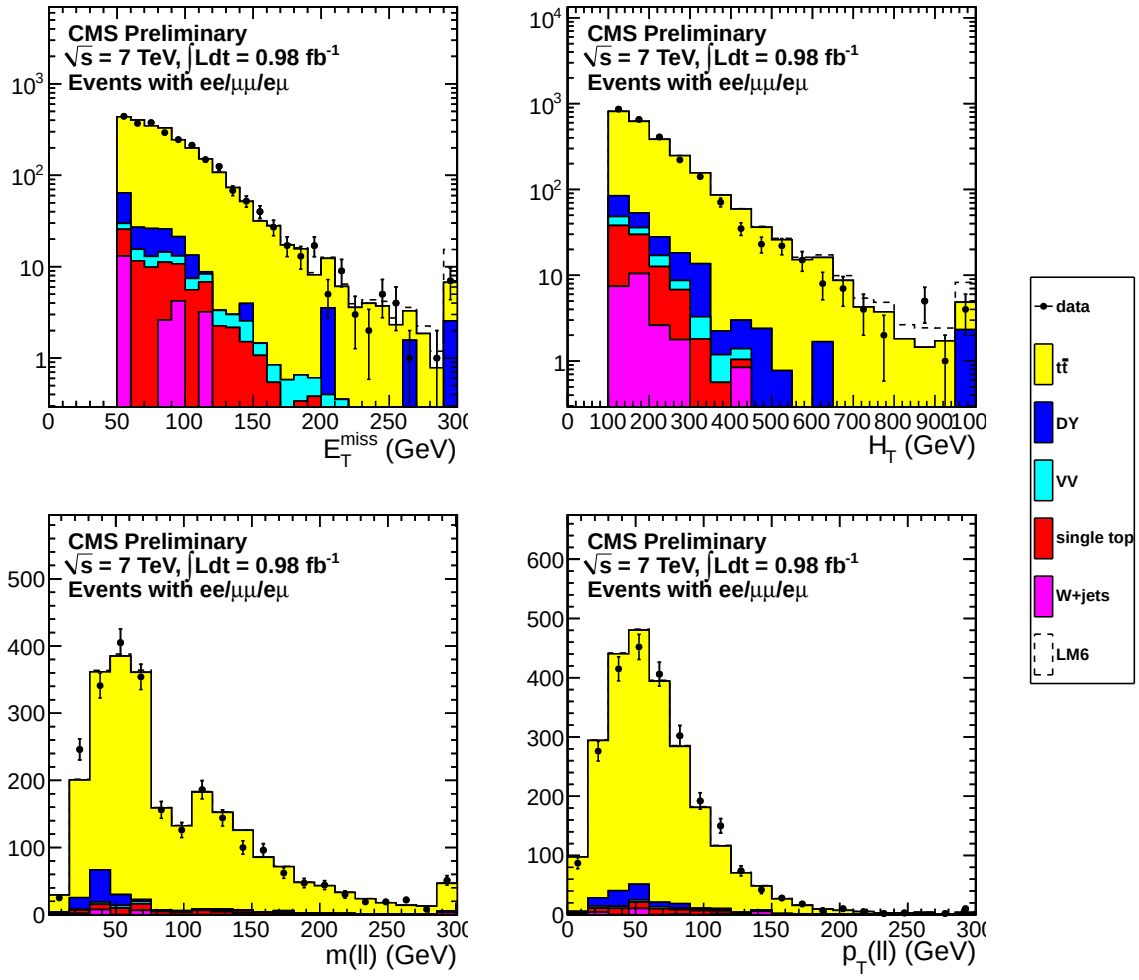

Figure 1: Distributions of (top left) missing tranverse energy $E_{\mathrm{T}}^{\mathrm{miss}}$, (top right) scalar sum of jet transverse energies (H_{T}), (bottom left) dilepton invariant mass $m(\ell\ell)$, and (bottom right) dilepton transverse momentum $p_{\mathrm{T}}(\ell\ell)$ for SM MC and data after preselection. The last bin contains the overflow. The MC has been normalized to match the data by applying a scale factor of 1.13. Here VV indicates the sum of WW, WZ, and ZZ. The MC distributions for the LM6 benchmark point are also shown.

4 Search for a Kinematic Edge

Any new physics process which produces leptons via a cascade decay chain will lead to final states containing same-flavor (SF) ee or $\mu\mu$ lepton pairs only, provided that lepton flavor is conserved. In contrast, for the dominant background $\mathrm{t\bar{t}}$ as well as other SM processes such as W^+W^- and DY $\rightarrow \tau^+\tau^-$, the 2 lepton flavors are uncorrelated, and the rates for SF and opposite-flavor (OF) $e\mu$ lepton pairs are therefore the same. Hence we can search for new physics in the SF final state, and model the backgrounds using events in the OF final state.

In Sec. 5 we search for an excess of events with SF with respect to OF lepton pairs, accompanied by large $E_{\mathrm{T}}^{\mathrm{miss}}$ and H_T. In this section, we search for a kinematic edge in the dilepton mass distribution for same-flavor events. This edge is a characteristic feature of, for example, SUSY scenarios in which the opposite-sign leptons are produced via the decay $\chi_2^0 \rightarrow \ell\tilde{\ell} \rightarrow \chi_1^0\ell^+\ell^-$. The $\mathrm{t\bar{t}}$ background shape is extracted from events with OF lepton pairs, and we perform a fit to

the dilepton mass distribution in events with SF lepton pairs.

Since we wish to examine the dilepton mass over the full range, in this section only we do not veto SF events in the Z mass region. This increases the DY contribution, and the $E_{\mathrm{T}}^{\mathrm{miss}}$ requirement is increased to $E_{\mathrm{T}}^{\mathrm{miss}} > 100$ GeV to compensate. We search for the kinematic edge in 2 regions. The first is a control region defined as $100 < H_T < 300$ GeV, which is dominated by the $\mathrm{t\bar{t}}$ background; we use this region to validate our fit methodology and verify that a signal yield consistent with 0 is obtained. We then proceed to search for a kinematic edge in the signal region defined as $H_T > 300$ GeV. Since we do not observe a kinematic edge in this region, we perform a fit to the dilepton mass distribution assuming an example signal shape from the LM1 scenario.

The contributions from fake leptons are treated as negligible, since they are measured to be roughly 1% of the total background using the data-driven fake rate technique. The residual DY contribution in the signal region is extrapolated from a control region at lower H_T, and is found to be negligible.

The background as a function of the invariant mass $m_{\ell\ell}$ is described by:

$$B(m_{\ell\ell}) = m_{\ell\ell}^{a} e^{-b m_{\ell\ell}}, \tag{1}$$

where $a \approx 1.5$ describes the rising edge and $b \approx 0.003$ dominates the long exponential tail on the right hand side of the shape. The extracted shape compared to the dilepton mass distribution in the control region for events containing OF lepton pairs is shown in Fig. 2 (upper-right).

For a potential signal, we use an edge model for two subsequent two-body decays, which comprises a triangular shape convoluted with a gaussian, according to:

$$T(m_{\ell\ell}) = \frac{1}{\sqrt{2\pi}\sigma_{ll}} \int_0^{M_{cut}} dy\, y e^{\frac{-(m_{\ell\ell}-y)^2}{2\sigma^2}}, \tag{2}$$

where the resolution parameters for electrons σ_{ee} and muons $\sigma_{\mu\mu}$ are constrained based on simulation.

The position of the kinematic edge M_{cut} is fixed based on the generator level information for the signal model which is tested; for example, for LM1 $M_{cut} = 78$ GeV. Finally, the Z contribution is modelled by a Breit-Wigner convoluted with a Gaussian (with fixed Z mass and width).

We perform a simultaneous, extended, unbinned maximum likelihood (ML) fit to the distribution of dilepton mass for events containing ee, $\mu\mu$ (signal, Z and background model) and $e\mu$ pairs (background model only). The shape of the $\mathrm{t\bar{t}}$ background is assumed to be common in all categories, and the yields of signal (n_S), Z (n_Z) and background (n_B) in these three categories are constrained using the ratio of muon to electron selection efficiencies $R_{\mu e} = 1.12 \pm 0.05$. This quantity is evaluated as the square root of the ratio of the number of $Z \to \mu^+\mu^-$ to $Z \to e^+e^-$ events in data, in the mass range 76-106 GeV with no jets or $E_{\mathrm{T}}^{\mathrm{miss}}$ requirements.

We perform the fit in the control region $100 < H_T < 300$ GeV, in which the $\mathrm{t\bar{t}}$ background, Z background, and LM1 signal yields are allowed to vary in the fit. The extracted signal yield, constrained to be positive, is $n_S = 10.7 \pm 15.4$, consistent with the background only hypothesis, as displayed in Fig. 2 (upper-left). The extracted Z yield is $n_Z = 7.3 \pm 6.1$, which is used to constrain the Z yield in the signal region.

Next, we perform the fit in the signal region $H_T > 300$ GeV. The $\mathrm{t\bar{t}}$ shape overlaid with OF

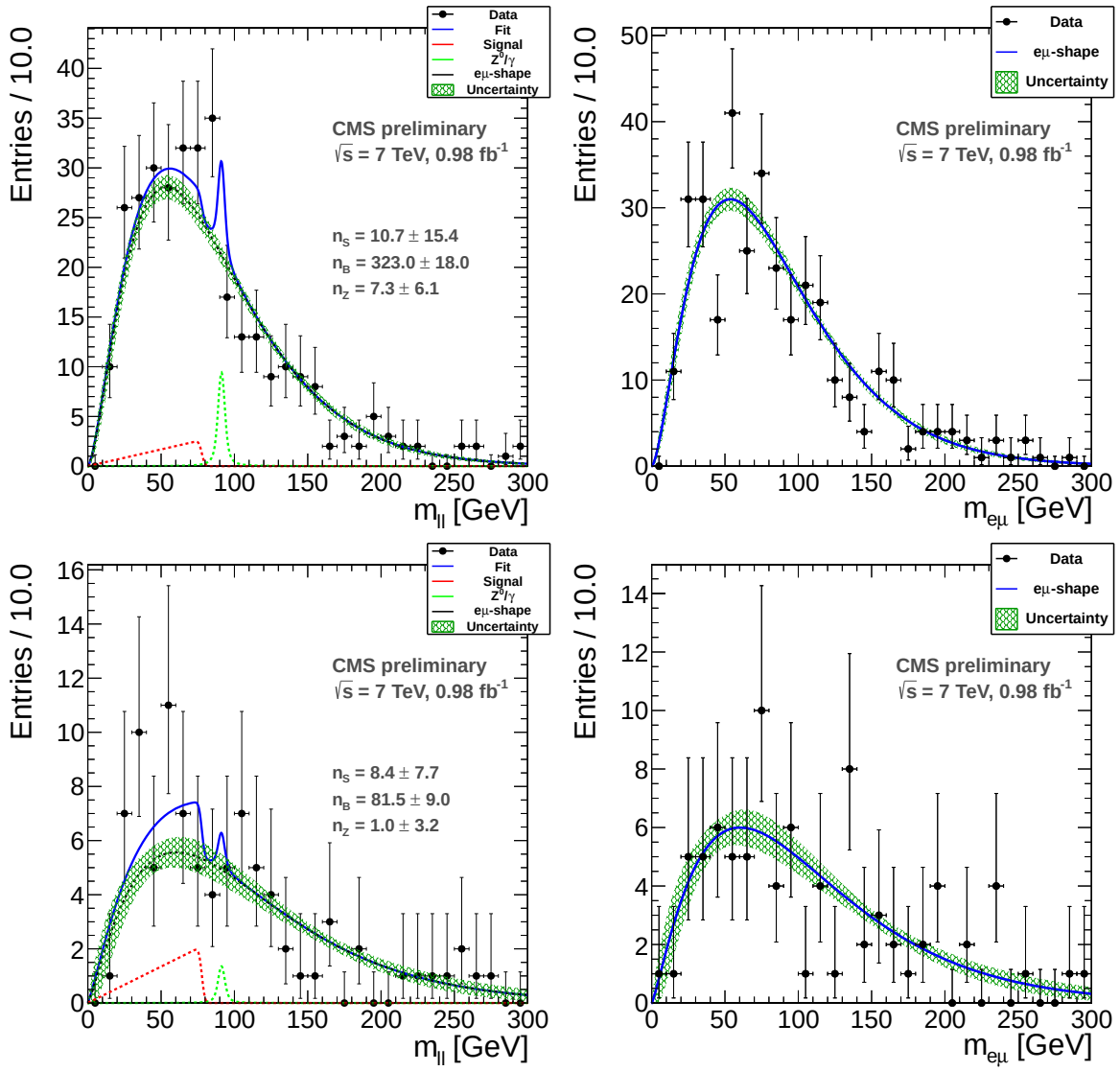

Figure 2: Results of the maximum likelihood fit to the dilepton mass distribution for events containing ee and $\mu\mu$ lepton pairs (left) and $e\mu$ lepton pairs (right) in the control region defined as $100 < H_T < 300$ GeV, $E_{\mathrm{T}}^{\mathrm{miss}} > 100$ GeV (upper) and the signal region $H_T > 300$ GeV, $E_{\mathrm{T}}^{\mathrm{miss}} > 100$ GeV (lower). In the extended fit the number of signal n_S, Z n_Z and $\mathrm{t\bar{t}}$ n_B events is extracted as well.

events is shown in Fig. 2 (lower-right). We constrain the Z yield in this region using an extrapolation in H_T from the control region $100 < H_T < 300$ GeV. The Z yield in the preselection region is multiplied by a scale factor from simulation corrected by a scale factor derived from Z events in data with no requirement on $E_{\mathrm{T}}^{\mathrm{miss}}$, which quantifies the fraction of Z events with $H_T > 100$ GeV which satisfy $H_T > 300$ GeV. Using this procedure we derive an upper limit on the Z yield in the signal region of $n_Z < 6.3$, which we use to constrain the Z yield in the ML fit. The extracted signal yield is $n_S = 8.4 \pm 7.7$, which is consistent with the background only hypothesis, as shown in Fig. 2 (lower-left). The expected LM1 yield in this region is 64 ± 6 events.

5 Counting Experiments

To look for possible BSM contributions, we define 2 signal regions that reject all but $\sim$0.1% of the dilepton $t\bar{t}$ events, by adding requirements of large $E_{\mathrm{T}}^{\mathrm{miss}}$ and H_T:

- high $E_{\mathrm{T}}^{\mathrm{miss}}$ signal region: $E_{\mathrm{T}}^{\mathrm{miss}} > 275$ GeV, $H_T > 300$ GeV,
- high H_T signal region: $E_{\mathrm{T}}^{\mathrm{miss}} > 200$ GeV, $H_T > 600$ GeV.

For the high $E_{\mathrm{T}}^{\mathrm{miss}}$ (high H_T) signal region, the SM MC predicts 7.3 (7.1) SM events, dominated by dilepton $t\bar{t}$; the expected LM1 yield is 49 (38), the expected LM3 yield is 18 (19), and the expected LM6 yield is 8.1 (7.4). The signal regions are indicated in Fig. 3. These signal regions are tighter than the one used in our published 2010 analysis since with the larger data sample they allow us to explore phase space farther from the core of the SM distributions.

We perform counting experiments in these signal regions, and use three independent methods to estimate from data the background in the signal region. The first method is a novel technique which is a variation of the ABCD method, which we used in our 2010 analysis [2], and exploits the fact that H_{T} and $y \equiv E_{\mathrm{T}}^{\mathrm{miss}}/\sqrt{H_T}$ are nearly uncorrelated for the $t\bar{t}$ background; this method is referred to as the ABCD' technique. First, we extract the y and H_T distributions $f(y)$ and $g(H_T)$ from data, using events from control regions which are dominated by background. Because y and H_T are weakly-correlated, the distribution of events in the y vs. H_T plane is described by:

$$\frac{\partial^2 N}{\partial y \partial H_T} = f(y)g(H_T), \tag{3}$$

allowing us to deduce the number of events falling in any region of this plane. In particular, we can deduce the number of events falling in our signal regions defined by requirements on $E_{\mathrm{T}}^{\mathrm{miss}}$ and H_T.

We measure the $f(y)$ and $g(H_T)$ distributions using events in the regions indicated in Fig. 4, and predict the background yields in the signal regions using Eq. 3. To estimate the statistical uncertainty in the predicted background, the bin contents of $f(y)$ and $g(H_T)$ are smeared according to their Poisson uncertainties. We have studied this technique using toy MC studies based on event samples of similar size to the expected yield in data for 1 fb^{-1}. Based on these studies we correct the predicted background yields by factors of 1.2 ± 0.2 (1.0 ± 0.2) for the high $E_{\mathrm{T}}^{\mathrm{miss}}$ (high H_T) signal region. These correction factors and uncertainties include the bias from the small correlation between H_T and y.

The second background estimate, henceforth referred to as the dilepton transverse momentum ($p_{\mathrm{T}}(\ell\ell)$) method, is based on the idea [18] that in dilepton $t\bar{t}$ events the p_{T} distributions of the charged leptons and neutrinos from W decays are related, because of the common boosts from the top and W decays. This relation is governed by the polarization of the W's, which is well understood in top decays in the SM [19, 20] and can therefore be reliably accounted for. We then use the observed $p_{\mathrm{T}}(\ell\ell)$ distribution to model the $p_{\mathrm{T}}(\nu\nu)$ distribution, which is identified with $E_{\mathrm{T}}^{\mathrm{miss}}$. Thus, we use the number of observed events with $H_{\mathrm{T}} > 300\,\mathrm{GeV}$ and $p_{\mathrm{T}}(\ell\ell) > 275\,\mathrm{GeV}$ ($H_{\mathrm{T}} > 600\,\mathrm{GeV}$ and $p_{\mathrm{T}}(\ell\ell) > 200\,\mathrm{GeV}$) to predict the number of background events with $H_{\mathrm{T}} > 300\,\mathrm{GeV}$ and $E_{\mathrm{T}}^{\mathrm{miss}} > 275\,\mathrm{GeV}$ ($H_{\mathrm{T}} > 600\,\mathrm{GeV}$ and $E_{\mathrm{T}}^{\mathrm{miss}} > 200\,\mathrm{GeV}$). In practice, we apply two corrections to this prediction, following the same procedure as in Ref. [2]. The first correction accounts for the fact that we require $E_{\mathrm{T}}^{\mathrm{miss}} > 50\,\mathrm{GeV}$ in the preselection but there is no corresponding requirement on $p_T(\ell\ell)$; this correction is $K_{50} = 1.5 \pm 0.3$ (1.3 ± 0.2) for the high $E_{\mathrm{T}}^{\mathrm{miss}}$ (high H_T) signal region. The second correction factor accounts for the W polarization in $\mathrm{t\bar{t}}$

events, as well as detector effects such as hadronic energy scale; this correction is $K_C = 1.5 \pm 0.5$ (1.3 ± 0.4) for the high $E_{\mathrm{T}}^{\mathrm{miss}}$ (high H_T) signal region.

Our third background estimation method is based on the fact that many models of new physics produce an excess of SF with respect to OF lepton pairs, while for the $\mathrm{t\bar{t}}$ background the rates of SF and OF lepton pairs are the same, as discussed in Sec. 4. Here we perform a counting experiment, by quantifying the excess of SF vs. OF pairs using the quantity

$$\Delta = R_{\mu e} N(ee) + \frac{1}{R_{\mu e}} N(\mu\mu) - N(e\mu), \tag{4}$$

with the muon to electron efficiency ratio $R_{\mu e} = 1.12 \pm 0.05$ introduced earlier.

This quantity is predicted to be 0 for processes with uncorrelated lepton flavors. In order for this technique to work, the kinematic selection applied to events in all dilepton flavor channels must be the same, which is not the case for our default selection because the Z mass veto is applied only to same-flavor channels. Therefore when applying the OF subtraction technique we also apply the Z mass veto to the $e\mu$ channel.

All background estimation methods based on data are in principle subject to signal contamination in the control regions, which tends to decrease the significance of a signal which may be present in the data by increasing the background prediction. In general, it is difficult to quantify these effects because we do not know what signal may be present in the data. Having three independent methods (in addition to expectations from MC) adds redundancy because signal contamination can have different effects in the different control regions for the three methods. For example, in the extreme case of a BSM signal with identical distributions of $p_{\mathrm{T}}(\ell\ell)$ and $E_{\mathrm{T}}^{\mathrm{miss}}$, an excess of events might be seen in the ABCD' method but not in the $p_{\mathrm{T}}(\ell\ell)$ method.

Backgrounds in which one or both leptons do not originate from electroweak decays (fake leptons) are assessed using the method of Ref. [9]. A fake lepton is a lepton candidate originating from within a jet, such as a lepton from semileptonic b or c decays, a muon decay-in-flight, a pion misidentified as an electron, or an unidentified photon conversion. We confirm the MC expectation that the fake lepton contribution is small compared to the dominant backgrounds. Estimates of the contributions to the signal region from pure multijet QCD, with two fake leptons, and in W + jets, with one fake lepton in addition to the lepton from the decay of the W, are derived separately. We find $0.0^{+0.4}_{-0.0}$ and 0.4 ± 0.4 ($0.00^{+0.4}_{-0.0}$ and 1.1 ± 0.7) for the multijet QCD and W+jets contributions to the high $E_{\mathrm{T}}^{\mathrm{miss}}$ (high H_T) signal regions, respectively, and thus consider these backgrounds to be negligible.

Backgrounds from DY are estimated with the data-driven $R_{out/in}$ technique [9], which leads to an estimated DY contribution which is consistent with 0. Backgrounds from processes with two vector bosons and single top are negligible compared to dilepton $t\bar{t}$.

6 Results of Counting Experiments

The data is displayed in the plane of $E_{\mathrm{T}}^{\mathrm{miss}}$ vs. H_T in Fig. 3. We find 8 (4) events in the high $E_{\mathrm{T}}^{\mathrm{miss}}$ (high H_T) signal regions, consistent with the MC expectations.

Next, we apply the ABCD' method to predict the yields in the high $E_{\mathrm{T}}^{\mathrm{miss}}$ and high H_T signal regions. The y vs. H_T distributions for data are displayed in Fig. 4. The signal regions are indicated, as well as the control regions used to measure the $f(y)$ and $g(H_T)$ distributions. For the high $E_{\mathrm{T}}^{\mathrm{miss}}$ (high H_T) signal region, we find a predicted yield of 4.0 ± 1.0 (stat) $\pm$ 0.8 (syst)

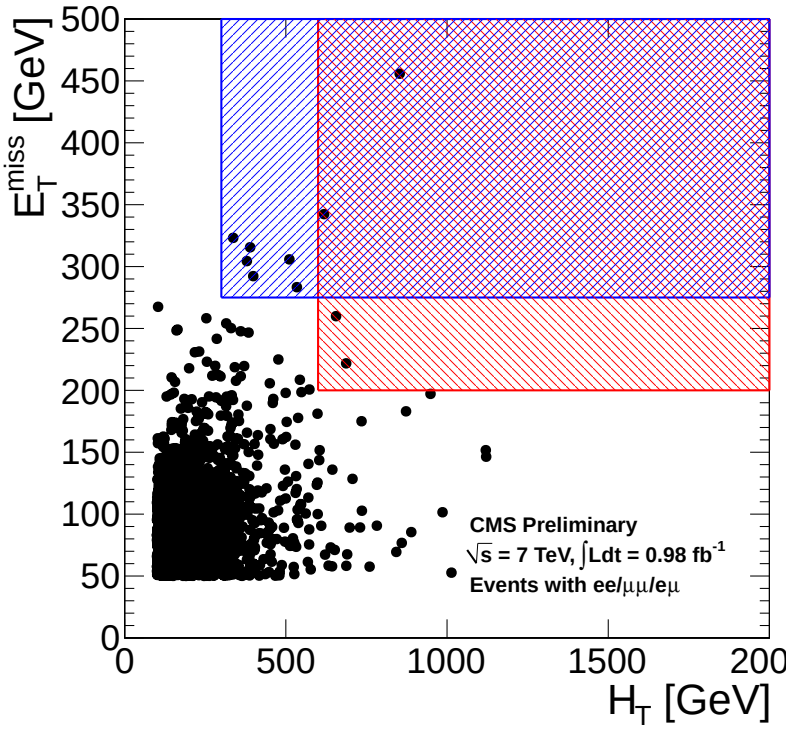

Figure 3: Distributions of $E_{\mathrm{T}}^{\mathrm{miss}}$ vs. H_{T} for data. The high $E_{\mathrm{T}}^{\mathrm{miss}}$ (high H_T) signal region is indicated with the blue dotted (red striped) region.

(4.5 $\pm$ 1.6 (stat) $\pm$ 0.9 (syst)), in reasonable agreement with the MC predictions and observed yields.

Next, we use the $p_T(\ell\ell)$ template method to predict the background in the 2 signal regions. For each signal region S, we count the number of events falling in the region S', which is defined using the same requirements as S but replacing the $E_{\mathrm{T}}^{\mathrm{miss}}$ requirement with a $p_T(\ell\ell)$ requirement. We subtract off the expected DY contribution to S' using the data-driven $R_{out/in}$ technique, and scale the corrected yield by the 2 correction factors K_{50} and K_C of Sec. 5.

The predicted and observed $E_{\mathrm{T}}^{\mathrm{miss}}$ distributions in the 2 signal regions are displayed in Fig. 5. For the high $E_{\mathrm{T}}^{\mathrm{miss}}$ (high H_T) signal regions we predict a background yield of 14.3 $\pm$ 6.3 (stat) $\pm$ 5.3 (syst) (10.1 $\pm$ 4.2 (stat) $\pm$ 3.5 (syst)) events, consistent with the observed yields and with the predictions of the ABCD' method.

As a validation of the $p_{\mathrm{T}}(\ell\ell)$ method in a region which is dominated by background, we also apply the $p_{\mathrm{T}}(\ell\ell)$ method in a control region by restricting H_{T} to be in the range 125–300 GeV. Here we predict 13.0 $\pm$ 6.1 (stat) $\pm$ 2.9 (syst) events with $E_{\mathrm{T}}^{\mathrm{miss}} > 200$ GeV, and observe 14 events in this region.

Our third background estimate is based on the OF subtraction technique. We observe 5 ee + 2 $e\mu$ (1 ee + 2 $e\mu$) events in the high $E_{\mathrm{T}}^{\mathrm{miss}}$ (high H_T) signal regions outside of the Z mass region 76–106 GeV. This gives $\Delta = 3.6 \pm 2.9$ (stat) $\pm$ 0.4 (syst) (-0.9 $\pm$ 1.8 (stat) $\pm$ 1.1 (syst))) for the high $E_{\mathrm{T}}^{\mathrm{miss}}$ (high H_T) signal regions, respectively, including the uncertainty in $R_{\mu e}$ and the uncertainty in the contribution from fake leptons.

A summary of our results is presented in Tables 2 and 3. For both signal regions, the observed yield is consistent with the predictions from MC and from the background estimates based on

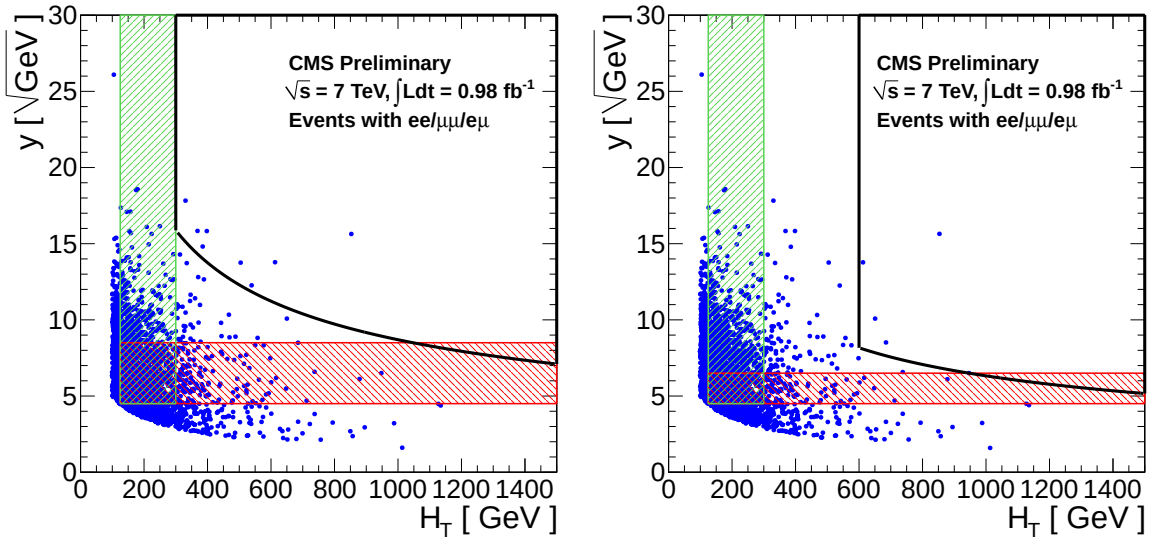

Figure 4: Distributions of y vs. H_T in data. The signal regions $E_{\mathrm{T}}^{\mathrm{miss}} > 275$ GeV, $H_T > 300$ GeV (left) and $E_{\mathrm{T}}^{\mathrm{miss}} > 200$ GeV, $H_T > 600$ GeV (right) are indicated with thick black lines. The $f(y)$ and $g(H_T)$ functions are measured using events in the green and red shaded areas, respectively.

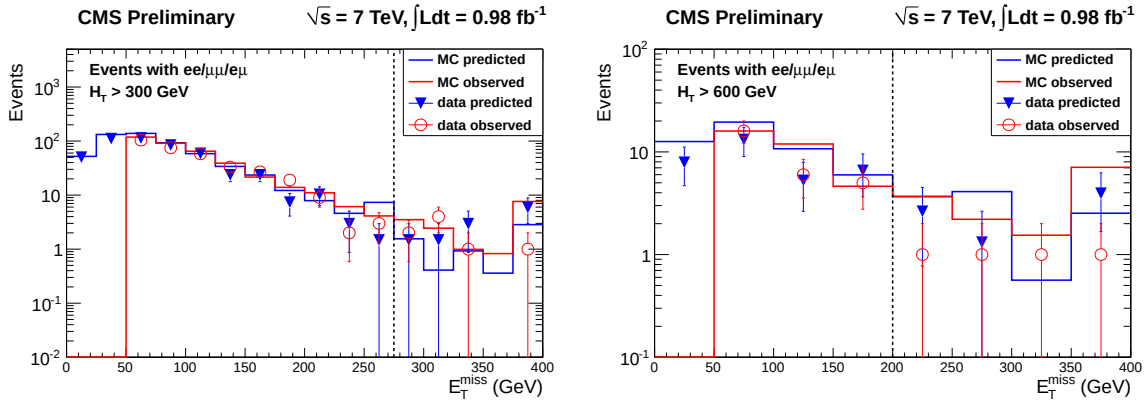

Figure 5: Distributions of $p_T(\ell\ell)$ scaled by the $E_{\mathrm{T}}^{\mathrm{miss}}$ acceptance correction factor K (predicted) and $E_{\mathrm{T}}^{\mathrm{miss}}$ (observed) for SM MC and data. The high $E_{\mathrm{T}}^{\mathrm{miss}}$ (high H_T) signal region is indicated by the vertical line in the left (right) plot.

data. We conclude that no evidence for non-SM contributions to the signal regions is observed.

Table 2: Summary of the observed and predicted yields in the 2 signal regions. The uncertainty in the MC prediction is statistical only. The systematic uncertainties on the ABCD′ and $p_T(\ell\ell)$ method predictions are discussed in the text. The background yield N_{bkg} is the error-weighted average of the 2 data-driven predictions. The non-SM yield UL is a CL_S 95% confidence level upper limit. The LM1, LM3 and LM6 yields include uncertainties from MC statistics, trigger efficiency, lepton selection efficiency, hadronic energy scale and integrated luminosity.

	high E_T^{miss} signal region	high H_T signal region
observed yield	8	4
MC prediction	7.3 ± 2.2	7.1 ± 2.2
ABCD′ prediction	4.0 ± 1.0 (stat) ± 0.8 (syst)	4.5 ± 1.6 (stat) ± 0.9 (syst)
$p_T(\ell\ell)$ prediction	14.3 ± 6.3 (stat) ± 5.3 (syst)	10.1 ± 4.2 (stat) ± 3.5 (syst)
N_{bkg}	4.2 ± 1.3	5.1 ± 1.7
non-SM yield UL	10	5.3
LM1	49 ± 11	38 ± 12
LM3	18 ± 5.0	19 ± 6.2
LM6	8.1 ± 1.0	7.4 ± 1.2

Table 3: Summary of the opposite-flavor subtraction results. The quantity Δ is defined in Eq. 4. The CL_S 95% CL upper limit on this quantity, as well as the predicted values in the LM1, LM3 and LM6 scenarios, are also summarized. The LM1, LM3 and LM6 uncertainties are from MC statistics, trigger efficiency, lepton selection efficiency, hadronic energy scale and integrated luminosity.

	high E_T^{miss} signal region	high H_T signal region
observed Δ	3.6 ± 2.9 (stat) ± 0.4 (syst)	-0.9 ± 1.8 (stat) ± 1.1 (syst)
UL	7.9	3.6
LM1	27 ± 6.0	24 ± 7.6
LM3	3.2 ± 0.9	3.3 ± 1.1
LM6	2.0 ± 0.2	1.9 ± 0.3

7 Acceptance and Efficiency Systematic Uncertainties

The acceptance and efficiency, as well as the systematic uncertainties in these quantities, depend on the signal model. For some of the individual uncertainties, it is reasonable to quote values based on SM control samples with kinematic properties similar to the SUSY benchmark models. For others that depend strongly on the kinematic properties of the event, the systematic uncertainties must be quoted model by model.

The systematic uncertainty in the lepton acceptance consists of two parts: the trigger efficiency uncertainty and the identification and isolation uncertainty. The trigger efficiency for two leptons of $p_{\mathrm{T}} > 10\,\mathrm{GeV}/c$, with one lepton of $p_{\mathrm{T}} > 20\,\mathrm{GeV}/c$ is measured using samples of $Z \to \ell\ell$, with an uncertainty of 2%. We verify that the MC reproduces the lepton identification and isolation efficiencies in data using samples of $Z \to \ell\ell$; the data and MC efficiencies are found to be consistent within 2%.

Another significant source of systematic uncertainty is associated with the jet and $E_{\mathrm{T}}^{\mathrm{miss}}$ energy scale. The impact of this uncertainty is final-state dependent. Final states characterized by very large hadronic activity and $E_{\mathrm{T}}^{\mathrm{miss}}$ are less sensitive than final states where the $E_{\mathrm{T}}^{\mathrm{miss}}$ and H_{T} are typically close to the minimum requirements applied to these quantities. To be more quantitative, we have used the method of Ref. [9] to evaluate the systematic uncertainties in the acceptance for $t\bar{t}$ and for the two benchmark SUSY points using a 7.5% uncertainty in the hadronic energy scale. The uncertainty on the LM1 signal efficiency in the region $H_T > 300$ GeV, $E_{\mathrm{T}}^{\mathrm{miss}} > 100$ GeV used to search for the kinematic edge is 5%. For the high $E_{\mathrm{T}}^{\mathrm{miss}}$ signal region for $t\bar{t}$ the uncertainty is $\sim$60%; for LM1, LM3 and LM6 the uncertainties are 22%, 27% and 10%, respectively. For the high H_T signal region for $t\bar{t}$ the uncertainty is $\sim$50%; for LM1, LM3 and LM6 the uncertainties are 30%, 32% and 14%, respectively.

The uncertainty in the integrated luminosity is 6% [21].

8 Limits on New Physics

We set an upper limit on the signal yield extracted by the fit to the dilepton mass distribution, assuming the LM1 shape. The 95% confidence level (CL) upper limit (UL) is extracted using a hybrid frequentist-bayesian $\mathrm{CL_S}$ method [22], giving an UL of 24.1 events, including uncertainties in the background yield and shape, resolution model and Z yield. In the limit setting we also include the uncertainties from trigger efficiency, lepton selection efficiency, hadronic energy scale and integrated luminosity on the signal efficiency. The expected LM1 yield is 64 ± 6 events. The $\mathrm{CL_S}$ 95% CL UL on cross-section times acceptance assuming a triangular signal shape and the LM1 signal efficiency and uncertainty is shown in Fig. 6.

We set upper limits on the non-SM contributions to the high $E_{\mathrm{T}}^{\mathrm{miss}}$ and high H_T signal regions. For both regions, we find reasonable agreement between the observed yields and the predictions from MC and from the ABCD' and $p_T(\ell\ell)$ data-driven methods. We extract $\mathrm{CL_S}$ 95% CL upper limits, where the background estimate is evaluated as the uncertainty-weighted average of the 2 data-driven background predictions, as summarized in Table 2. These generic upper limits are not corrected for the possibility of signal contamination in the control regions. This is justified because the two independent background estimation methods based on data are consistent and are also consistent with the SM MC prediction. Moreover, no evidence for non-SM contributions in the control regions is observed (Table 1 and Fig. 1). The results of the search for correlated flavor dilepton production using the opposite-flavor subtraction technique are summarized in Table 3. We set a $\mathrm{CL_S}$ 95% CL upper limit on the quantity Δ and compare this

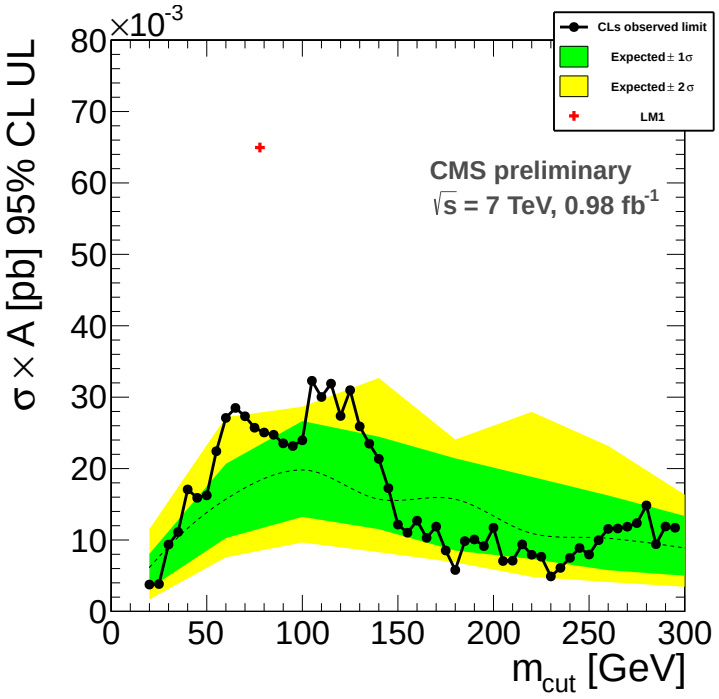

Figure 6: CL_S 95% confidence level upper limit on cross-section times acceptance as a function of the endpoint in the invariant mass spectrum assuming a triangular shaped signal.

to the predicted values in the LM1, LM3 and LM6 scenarios. For the specific benchmark SUSY processes considered in this note, the results of the inclusive search achieve higher sensitivity than the results of the correlated flavor search. These results significantly extend the sensitivity of our previous 2010 results [2].

The results of the counting experiments in the high $E_{\mathrm{T}}^{\mathrm{miss}}$ and high H_T signal regions are also used to place model-dependent limits on the quantity $\sigma \times A$ for the benchmark processes LM1, LM3 and LM6. Here σ is the NLO cross-section and the acceptance is defined by the following requirements, applied to the generator-level quantities. We require the presence of at least 2 opposite-sign leptons (electrons or muons) with $p_{\mathrm{T}} > 10$ GeV and $|\eta| < 2.5$; at least 1 of the leptons must have $p_{\mathrm{T}} > 20$ GeV, and same-flavor lepton pairs with $76 < m(\ell\ell) < 106$ GeV are vetoed. We require at least 2 generator-level jets with $p_{\mathrm{T}} > 30$ GeV and $|\eta| < 3.0$, separated by $\Delta R > 0.4$ from any lepton passing the above selection; the generator-level H_T is the scalar sum of the transverse energies of these selected jets. The generator-level $E_{\mathrm{T}}^{\mathrm{miss}}$ is the vector sum of the transverse momenta of the invisible neutrinos and LSP's. For each signal region we include the corresponding requirements on the generator-level $E_{\mathrm{T}}^{\mathrm{miss}}$ and H_T. The efficiency is defined with respect to events passing this acceptance selection. We place CL_S 95% UL's on the quantity $\sigma \times A$, and compare these limits to the expected values of this quantity for the 3 benchmark SUSY scenarios. The results are summarized in Table 4, which indicates that all 3 benchmark SUSY scenarios are ruled out by these results.

We also quote the result more generally in the context of the CMSSM. The CL_S 95% CL limit in the $(m_0, m_{1/2})$ plane, for $\tan\beta = 10$, $A_0 = 0$ and $\mu > 0$ is shown in Figure 7. The high $E_{\mathrm{T}}^{\mathrm{miss}}$ and high H_T signal regions have similar sensitivity to the CMSSM; here we choose to show results based on the high H_T signal region. The SUSY particle spectrum is calculated using SoftSUSY [23], and the signal events are generated at leading order (LO) with PYTHIA 6.4.22. NLO cross sections, obtained with the program Prospino [24], are used to calculate the

Table 4: Summary of model-dependent limits. The efficiency and acceptance are defined in the text; the efficiency uncertainty is dominated by the uncertainty in the hadronic energy scale. The CL_S 95% CL UL on the quantity $\sigma \times A$ is indicated, as well as the value of this quantity for the LM1, LM3 and LM6 scenarios.

	LM1	LM3	LM6
high E_T^{miss} signal region			
efficiency (%)	45 ± 10	41 ± 11	52 ± 6
acceptance (%)	1.6	0.84	3.3
UL($\sigma \times A$) (fb)	25	28	20
$\sigma \times A$ (fb)	108	43	16
high H_T signal region			
efficiency (%)	42 ± 13	38 ± 12	50 ± 7
acceptance (%)	1.2	0.85	3.0
UL($\sigma \times A$) (fb)	15	17	12
$\sigma \times A$ (fb)	83	46	15

observed exclusion contour. At each point in the $(m_0, m_{1/2})$ plane, the acceptance uncertainty is calculated by summing in quadrature the uncertainties from jet and E_T^{miss} energy scale using the procedure discussed in Section 7, the uncertainty in the NLO cross section due to the choice of factorization and renormalization scale, and the uncertainty from the parton distribution functions and α_S, evaluated using the prescription from the PDF4LHC recommendation [25]. The luminosity, trigger efficiency, and lepton selection efficiency uncertainties are also included, giving a total relative acceptance uncertainty which varies in the range ~0.3–0.4. A point is considered to be excluded if the NLO yield exceeds the CL_S 95% CL upper limit calculated with this acceptance uncertainty.

The excluded regions for the CDF search for jets + missing energy final states [26] were obtained for $\tan\beta = 5$, while those from D0 [27] were obtained for $\tan\beta = 3$, each with approximately 2 fb^{-1} of data and for $\mu < 0$. The LEP-excluded regions are based on searches for sleptons and charginos [28]. The D0 exclusion limit, valid for $\tan\beta = 3$ and obtained from a search for associated production of charginos $\chi_1^\pm$ and neutralinos χ_2^0 in trilepton final states [29], is also included in Figure 7. In contrast to the other limits presented in Figure 7, the results of our search and of the trilepton search are strongly dependent on the choice of $\tan\beta$ and they reach the highest sensitivity in the CMSSM for $\tan\beta$ values below 10.

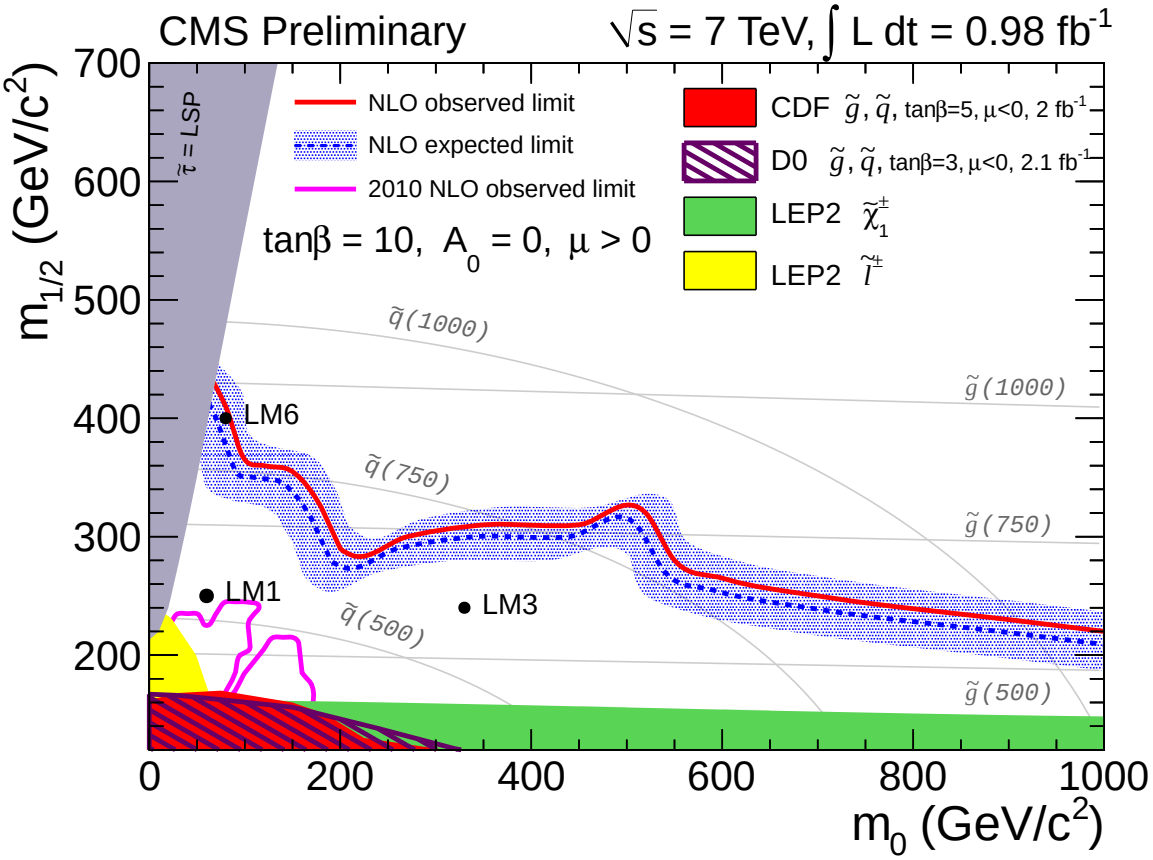

Figure 7: The observed 95% CL exclusion contour at NLO (solid red line) and the expected exclusion contour (dashed blue line) with $\pm 1\sigma$ variation (shaded blue region) in the CMSSM $(m_0, m_{1/2})$ plane for $\tan\beta = 10$, $A_0 = 0$ and $\mu > 0$. The area below the curve is excluded by this measurement. Exclusion limits obtained from previous experiments are presented as filled areas in the plot. Thin grey lines correspond to constant squark and gluino masses. This exclusion is based on the results of the high H_T signal region, for which the observed yield is 4 events and the expected background yield is 5.1 ± 1.7 events. The exclusion contour based on 34 pb^{-1} 2010 data is also displayed.

9 Additional Information for Model Testing

Other models of new physics in the dilepton final state can be confronted in an approximate way by simple generator-level studies that compare the expected number of events in $0.98\,\text{fb}^{-1}$ with the upper limits from Section 8. The key ingredients of such studies are the kinematic requirements described in this note, the lepton efficiencies, and the detector responses for H_T and E_T^miss. The trigger efficiencies for events containing ee, $e\mu$ or $\mu\mu$ lepton pairs are 100%, 95%, and 90%, respectively. The muon identification efficiency is $\approx$ 96%; the electron identification efficiency varies approximately linearly from $\approx$ 60% at $p_\text{T} = 10\,\text{GeV}/c$ to 90% for $p_\text{T} > 30\,\text{GeV}/c$. The lepton isolation efficiency depends on the lepton momentum, as well as on the jet activity in the event. In $t\bar{t}$ events, it varies approximately linearly from $\approx$ 73% (muons) and $\approx$ 82% (electrons) at $p_\text{T} = 10\,\text{GeV}/c$ to $\approx$ 97% for $p_\text{T} > 60\,\text{GeV}/c$. In LM1 (LM3) events, this efficiency is decreased by $\approx$5–10% ($\approx$10%,$\approx$5%)over the whole momentum spectrum. The average detector responses (the reconstructed quantity divided by the generated quantity) for H_T and E_T^miss are consistent with 1 within the 7.5% jet energy scale uncertainty. The experimental resolutions on these quantities are 9% and 12%, respectively.

10 Summary

We have presented a search for BSM physics in the opposite-sign dilepton final state using a data sample of proton-proton collisions at 7 TeV centre-of-mass energy corresponding to an integrated luminosity of $0.98\,\text{fb}^{-1}$, recorded by the CMS detector in 2011. Two complementary search strategies were performed. The first focused on models with a specific dilepton production mechanism leading to a characteristic kinematic edge in the dilepton mass distribution, and the second focused on dilepton events accompanied by large missing transverse energy and significant hadronic activity, motivated by many models of BSM physics, such as supersymmetric models. In the absence of evidence for BSM physics, we have set upper limits on the non-SM contributions to yields in the signal regions. Additional information was provided to allow testing whether specific models of new physics are excluded by these results.

References

[1] CMS Collaboration, "The CMS experiment at the CERN LHC", *JINST* **3** (2008) S08004. doi:10.1088/1748-0221/3/08/S08004.

[2] CMS Collaboration Collaboration, "Search for Physics Beyond the Standard Model in Opposite-Sign Dilepton Events at $\sqrt{s} = 7$ TeV", arXiv:1103.1348. * Temporary entry *.

[3] G. Bertone, D. Hooper, and J. Silk, "Particle dark matter: Evidence, candidates and constraints", *Phys.Rept.* **405** (2005) 279–390, arXiv:hep-ph/0404175. doi:10.1016/j.physrep.2004.08.031.

[4] H. Baer, "TASI 2008 lectures on Collider Signals. II. Missing E(T) signatures and the dark matter connection", arXiv:0901.4732.

[5] S. P. Martin, "A Supersymmetry primer", arXiv:hep-ph/9709356.

[6] J. Wess and B. Zumino, "Supergauge Transformations in Four-Dimensions", *Nucl.Phys.* **B70** (1974) 39–50. doi:10.1016/0550-3213(74)90355-1.

[7] CMS Collaboration Collaboration, "Search for Supersymmetry in pp Collisions at 7 TeV in Events with Jets and Missing Transverse Energy", *Phys.Lett.* **B698** (2011) 196–218, arXiv:1101.1628. * Temporary entry *. doi:10.1016/j.physletb.2011.03.021.

[8] CMS Collaboration Collaboration, "Search for new physics with same-sign isolated dilepton events with jets and missing transverse energy at the LHC", arXiv:1104.3168.

[9] CMS Collaboration Collaboration, "First Measurement of the Cross Section for Top-Quark Pair Production in Proton-Proton Collisions at sqrt(s)=7 TeV", *Phys.Lett.* **B695** (2011) 424–443, arXiv:1010.5994. doi:10.1016/j.physletb.2010.11.058.

[10] G. L. Kane, C. F. Kolda, L. Roszkowski et al., "Study of constrained minimal supersymmetry", *Phys.Rev.* **D49** (1994) 6173–6210, arXiv:hep-ph/9312272. doi:10.1103/PhysRevD.49.6173.

[11] A. H. Chamseddine, R. L. Arnowitt, and P. Nath, "Locally Supersymmetric Grand Unification", *Phys.Rev.Lett.* **49** (1982) 970. doi:10.1103/PhysRevLett.49.970.

[12] CMS Collaboration, "CMS technical design report, volume II: Physics performance", *J. Phys. G* **34** (2007) 995–1579. doi:10.1088/0954-3899/34/6/S01.

[13] T. Sjostrand, S. Mrenna, and P. Z. Skands, "PYTHIA 6.4 Physics and Manual", *JHEP* **0605** (2006) 026, arXiv:hep-ph/0603175. doi:10.1088/1126-6708/2006/05/026.

[14] J. Alwall, "MadGraph/MadEvent v4: The New Web Generation", *JHEP* **2007** (2007) 028. doi:10.1088/1126-6708/2007/09/028.

[15] GEANT4 Collaboration, "GEANT4: A Simulation toolkit", *Nucl.Instrum.Meth.* **A506** (2003) 250–303. doi:10.1016/S0168-9002(03)01368-8.

[16] M. Cacciari, G. P. Salam, and G. Soyez, "The Anti-k(t) jet clustering algorithm", *JHEP* **0804** (2008) 063, arXiv:0802.1189. doi:10.1088/1126-6708/2008/04/063.

[17] CMS Collaboration, "Commissioning of the Particle-Flow Reconstruction in Minimum-Bias and Jet Events from pp Collisions at 7 TeV", *CMS Physics Analysis Summary* **CMS-PAS-PFT-10-002** (2010).

[18] V. Pavlunin, "Modeling missing transverse energy in V+jets at CERN LHC", *Phys.Rev.* **D81** (2010) 035005, arXiv:0906.5016. doi:10.1103/PhysRevD.81.035005.

[19] J. Aguilar-Saavedra, J. Carvalho, N. F. Castro et al., "Probing anomalous Wtb couplings in top pair decays", *Eur.Phys.J.* **C50** (2007) 519–533, arXiv:hep-ph/0605190. doi:10.1140/epjc/s10052-007-0289-4.

[20] A. Czarnecki, J. G. Korner, and J. H. Piclum, "Helicity fractions of W bosons from top quark decays at NNLO in QCD", *Phys.Rev.* **D81** (2010) 111503, arXiv:1005.2625. doi:10.1103/PhysRevD.81.111503.

[21] CMS Collaboration, "Measurement of CMS Luminosity", *CMS Physics Analysis Summary* **CMS-PAS-EWK-10-002** (2010).

[22] Particle Data Group Collaboration, "Review of particle physics", *J. Phys.* **G 37** (2010) 075021. doi:10.1088/0954-3899/37/7A/075021.

[23] B. Allanach, "SOFTSUSY: a program for calculating supersymmetric spectra", *Comput.Phys.Commun.* **143** (2002) 305. doi:10.1016/S0010-4655(01)00460-X.

[24] W. Beenakker et al., "Squark and Gluino Production at Hadron Colliders", *Nucl.Phys.* **B492** (1997) 51. doi:10.1016/S0550-3213(97)00084-9.

[25] M. Botje, J. Butterworth, A. Cooper-Sarkar et al., "The PDF4LHC Working Group Interim Recommendations", arXiv:1101.0538.

[26] CDF Collaboration, "Inclusive Search for Squark and Gluino Production in $p\bar{p}$ Collisions at $\sqrt{s} = 1.96$ *TeV*", *Phys. Rev. Lett.* **102** (Mar, 2009) 121801. doi:10.1103/PhysRevLett.102.121801.

[27] D0 Collaboration, "Search for squarks and gluinos in events with jets and missing transverse energy using 2.1 fb^{-1} of collision data at $\sqrt{s} = 1.96$ TeV", *Physics Letters B* **660** (2008) 449. doi:10.1016/j.physletb.2008.01.042.

[28] LEPSUSYWG, ALEPH, DELPHI, L3 and OPAL experiments, "LSP mass limit in Minimal SUGRA",. LEPSUSYWG/02-06.2.

[29] D0 Collaboration, "Search for associated production of charginos and neutralinos in the trilepton final state using 2.3 fb^{-1} of data", *Physics Letters B* **680** (2009) 34. doi:10.1016/j.physletb.2009.08.011.